

pubs.acs.org/JPCC Article

Electrically Driven Magnetization Reorientation at the Fe/PbTiO₃ Interface

Tumentsereg Ochirkhuyag, Nicholas Kioussis, Sonny H. Rhim, and Dorj Odkhuu*



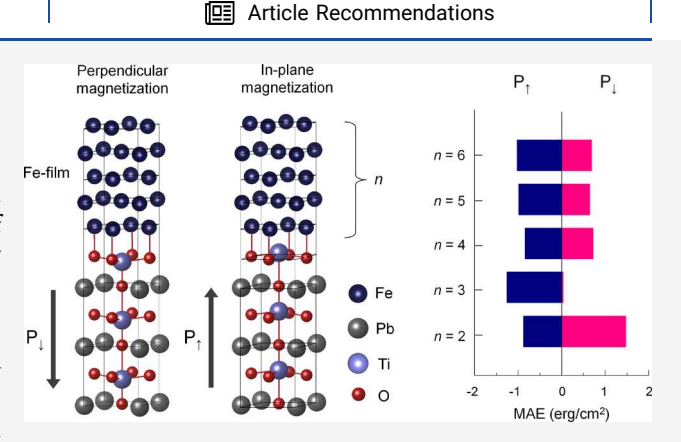
Cite This: J. Phys. Chem. C 2023, 127, 24467-24474



ACCESS I

Metrics & More

ABSTRACT: Employing first-principles electronic structure calculations, we investigate the thermodynamic stability, magnetization, and magnetic anisotropy energy (MAE) at the interface between the ultrathin Fe(001) and PbTiO₃(001) (PTO) layers. Herein we demonstrate the ferroelectric polarization driven magnetization reorientation at the Fe/PTO interface. Changes in energy levels of the strong spin—orbit coupled Fe 3d and Pb 6p orbital states under the reversible ferroelectric polarization of Ti displacement are responsible for the magnetization reorientation at the Fe/PTO interface. Furthermore, we reveal that magnetization reversal persists for Fe-film thicknesses of >1 nm and even under a practically achievable strain of 1%. The present study provides a viable route for achieving the electric-field-only manipulation of magnetization switching in magnetoelectric spintronics.



INTRODUCTION

Exploration for epitaxial atomistic interfaces that exhibit physical properties not found in their constituent materials dates back a few decades. One of the most profound cases is the magnetoelectric coupling that occurs at the interface between the ferroelectric (FE) and magnetic (ferromagnetic, FM, and antiferromagnetic, AFM) layers owing to the interplay between charge and spin degrees of freedom. Ab initio studies reported that the interfaces between the BaTiO3 or SrTiO3 and Fe or FeRh layers can exhibit an electric polarization reversal induced change in magnetism and magnetocrystalline anisotropy (MCA).¹⁻³ These phenomena have provided a new concept in the research area of electric-field control of magnetism, which offers a viable path to electrically addressable magnetic memories in spintronics.^{4,5} Nevertheless, the recent development of magnetoelectric memory technologies requires a breakthrough leading to the electrical switching of magnetization in the absence of a magnetic-field or spin-transfer torque effect (STT).6 An ideal FM/FE interface that can fulfill this prerequisite has been exceptionally uncommon. The main obstacle, despite many research efforts, 7-10 is commonly regarded as a relatively weak magnetoelectric effect, which is insufficient to overcome the energy barrier to reorient magnetic moments, i.e., magnetic anisotropy energy (MAE). Recently, the adoption of highly polarized ferroelectrics, mainly PbTiO3 based materials, is shown to enhance the strength of magnetoelectric coupling.11-13

In this paper, using density functional theory (DFT) calculations, we explore the possibility of the magnetization switching at the Fe/PbTiO_3 (or Fe/PTO) interface by means of the ferroelectric polarization. The reversible polarization of the Ti displacement alters energy levels of the strong spinorbit coupled Fe 3d and Pb 6p orbital states at the Fe/PTO interface, which in turn leads to the magnetization reorientation. It is further predicted that this magnetization reorientation persists under a practically achievable strain of 1% but is limited to a certain film thickness of Fe layers, which is determined by the competition between the MCA and shape anisotropy (K_s) contributions to MAE. Moreover, density functional perturbation theory (DFPT) simulations demonstrate that the Fe/PTO interface is thermodynamically stable.

COMPUTATIONAL METHODS

The DFT and DFPT simulations were performed using the Vienna *ab initio* simulation package (VASP)^{14,15} version 5.4.4. Exchange–correlation functional is treated with the generalized gradient approximation (GGA) by Perdew, Burke, and Ernzerhof (PBE).¹⁶ Our model geometries consist of 2–6

Received: October 13, 2023 Revised: November 9, 2023 Accepted: November 17, 2023 Published: December 12, 2023





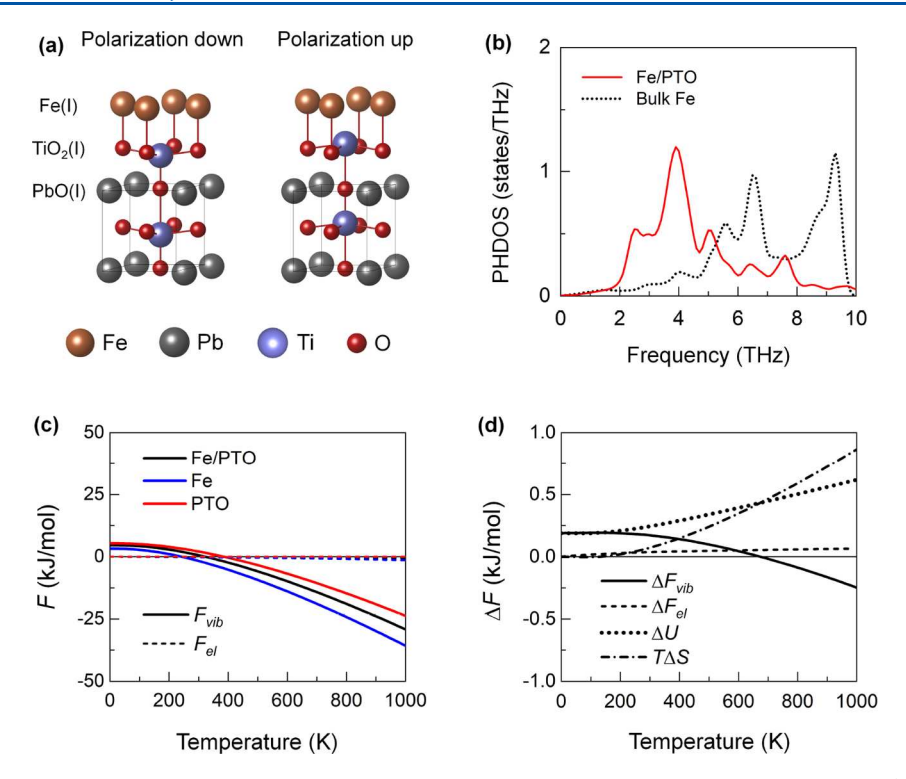


Figure 1. (a) Schematic atomic structures representing the Fe/PTO interface for the ferroelectric polarization down (left) and polarization up (right), where only the interface (I) Fe and PTO layers are shown. Brown, gray, blue, and red spheres represent the Fe, Pb, Ti, and O atoms, respectively. (b) Phonon density of states (PHDOS) of the Fe atom at the Fe/PTO interface. For comparison, the same for bulk Fe is also shown in the dotted line. (c) Free energy contributions of $F_{\rm el}(T,V)$ and $F_{\rm vib}(T,V)$ and $F_{\rm vib}(T,V)$ and $F_{\rm vib}(T,V)$ are also shown.

atomic layers (n) of Fe films deposited on the 9 unit cell (uc) of PTO (BaTiO₃ or BTO) and a vacuum region no less than 12 Å along the z axis. Figure 1a shows the schematic interface between the Fe and the PTO layers. We adapted an in-plane lattice parameter of Fe/PTO supercell to the optimized lattice constant (3.845 Å) of bulk PTO, where the lattice mismatch with Fe (~4%) is comparable to an experimental value of 3.68%. There is no lattice mismatch between the Fe and BTO layers; the optimized lattice constant (4.00 Å) of bulk BTO agrees well with the experimental value of 4.00 Å. For both Fe/PTO and Fe/BTO, Fe atoms are favored on top of the O sites at the TiO2 interface, in agreement with an experiment. 19 Ionic positions of all Fe atoms and 4 uc layers of PTO (BTO) next to the interface were fully relaxed while the bottommost 5 uc layers were kept fixed with their bulk polarization in the negative (P_{\downarrow}) and positive z directions (P_{\uparrow}) to retain ferroelectricity (Figure 1a).²⁰ An energy cutoff of 500 eV and a $11 \times 11 \times 1$ k point mesh were imposed for the ionic relaxation, where the forces acting on each atom were less than 10^{-2} eV/Å. The MCA is calculated based on the total energy difference when the magnetization directions are in the xyplane (E^{\parallel}) and along the z axis (E^{\perp}) , MCA = $(E^{\parallel} - E^{\perp})/A$, where *A* is the area of the interface. To obtain reliable values of MCA, the Gaussian smearing method with a smaller smearing of 0.05 and dense k points of 25 \times 25 \times 1 were used in noncollinear calculations, where the spin-orbit coupling (SOC) term was included using the second-variation method employing the scalar-relativistic eigenfunctions of the valence states. The surface shape anisotropy K_s is determined from Bruno's expression, $K_s = -(1/2)M_vM_{s}^{22}$ where M_v is the bulk magnetization per unit volume and M_s is the sum of excess surface magnetization per unit area for each layer. Phonon

dispersion and thermodynamic properties were carried out by using the PHONOPY code²³ within the harmonic approximation in the DFPT scheme.²⁴ For the phonon calculations, we employed a 2×2 lateral supercell and a $3 \times 3 \times 1$ k-point mesh in the interpolation of force constant matrices.

RESULTS AND DISCUSSION

In order for Fe/PTO to be practical, we first inspect the thermodynamic stability at the Fe/PTO interface. The Helmholtz free energy can be written as $F(T,V)=E_0(V)+F_{\rm el}(T,V)+F_{\rm vib}(T,V)$, where $E_0(V)$ is the zero-temperature total energy of the system and $F_{\rm el}(T,V)$ and $F_{\rm vib}(T,V)$ are the electronic and vibrational contributions of the free energy, respectively. The vibrational contribution to the free energy is described by $F_{\rm vib}(T,V)=U(T,V)-TS(T,V)$, where U(T,V) is the internal energy of the lattice including zero point vibrations and S(T,V) is the entropy of the system. The thermodynamic stability of the Fe/PTO bilayer against decomposition into the Fe and PTO component layers can be described mainly by the change in the vibrational free energy: 25,26 $\Delta F_{\rm vib}(P,V)=F_{\rm vib}^{\rm Fe/PTO}(T,V)-F_{\rm vib}^{\rm Fe}(T,V)-F_{\rm vib}^{\rm Fe}(T,V)$, where $F_{\rm vib}^{\rm Fe/PTO}(T,V)$, $F_{\rm vib}^{\rm Fe}(T,V)$, and $F_{\rm vib}^{\rm PTO}(T,V)$ are the vibrational free energies of the Fe/PTO, Fe, and PTO layers, respectively.

In Figure 1b we present the phonon density of states (PHDOS) of the Fe atom at the Fe/PTO interface in comparison with bulk Fe. In the phonon calculations (which are computationally expensive), only the 2 uc PTO and no reversible ferroelectric polarization effects are taken into account, which we believe do not change explicitly our conclusion on the interface stability. Note that here and hereafter our results correspond to those for Fe-film thickness

Table 1. Relative Displacements (Å) of the Fe, Ti, and Pb/Ba Atoms with Respect to the O-Plane and the Polarization P_z (μ C cm⁻²) along the z Axis at the Fe/PTO and Fe/BTO Interfaces (n = 5) and in Bulk PTO and BTO for the Ferroelectric Polarization Down P_{\perp} and Polarization Up P_{\uparrow}^a

	Fe-O		Ti-O		Pb/Ba	а-О	P_z (present)		
	P_{\downarrow}	P_{\uparrow}	P_{\downarrow}	P_{\uparrow}	P_{\downarrow}	P_{\uparrow}	P_{\downarrow}	P_{\uparrow}	P_z (exp)
Fe/PTO	1.89	2.07	-0.50	0.32	-0.83	0.63	84.5	59.2	
bulk PTO			-0.52	0.52	-0.88	0.88	88.7	88.7	83 ^b
Fe/BTO	1.93	1.92	-0.17	0.08	-0.18	0.11	24.4	12.5	
bulk BTO			-0.18	0.18	-0.19	0.19	28.9	28.9	26 ^c

^aFor comparison, we also show the experimental results of P_z for PTO and BTO.^{33,34} ^bReference 33. ^cReference 34.

Table 2. Calculated Magnetic Moment (μ_B) and Relative Charge with Respect to the Nominal Charge (e) of the Fe, Ti, Pb/Ba, and O Atoms at the Fe/PTO and Fe/BTO Interfaces for the Ferroelectric Polarization Down P_{\downarrow} and Polarization Up P_{\uparrow}

			magnetic	moment		charge				
		Fe	Ti	Pb/Ba	0	Fe	Ti	Pb/Ba	О	
Fe/PTO	P_{\downarrow}	2.85	0.04	0.00	0.08	-0.43	-2.51	0.13	1.30	
	P_{\uparrow}	2.46	-0.54	0.02	0.03	-0.06	-2.19	0.35	1.48	
Fe/BTO	P_{\downarrow}	2.76	0.02	0.00	0.07	-0.34	-2.41	0.44	1.38	
	P_{\uparrow}	2.61	-0.60	0.00	0.05	-0.24	-2.23	0.45	1.40	

of 5 atomic layers (n = 5), unless specifically mentioned. As shown in Figure 1b, the interface Fe exhibits lower vibrational frequencies compared with those in bulk Fe, which is associated with the reduced number of Fe–Fe bonds.²⁷ Nevertheless, no imaginary frequency modes exist in the phonon dispersion. A similar finding is reported in previous Fe(001)-film calculations.^{27,28}

Figure 1c shows the free energy contributions of $F_{\rm el}(T, V)$ and $F_{vib}(T, V)$ as a function of temperature for the Fe/PTO, Fe, and PTO layers. The temperature dependent $\Delta F_{\rm el}(T, V)$ and $\Delta F_{\text{vib}}(T, V)$ values along with $\Delta U(T, V)$ and $T\Delta S(T, V)$ values are also plotted in Figure 1d. In the temperaturedependent free energy calculations, the in-plane lattice parameter of the Fe/PTO structure is kept fixed at its optimized value obtained from the DFT calculations. Both F(T, V) and $\Delta F(T, V)$ are mainly accounted for by the vibrational contribution, while the electronic contribution is insignificant. As a generic for all systems, $F_{vib}(T, V)$ decreases as temperature increases, where $F_{\rm vib}(T,\,V)$ values of Fe layers are lower compared with those for the other two compounds throughout the temperature range owing to the good thermal stability of Fe films. The computed $\Delta F(T, V)$ value of the Fe/ PTO interface is approximately -7.4 kJ mol⁻¹ (or -0.08 eV atom⁻¹) at 0 K and decreases further with the temperature associated with $\Delta F_{\text{vib}}(T, V)$ (solid line in Figure 1d). Hence, the Fe/PTO interface is predicted to be thermodynamically stable. We expect a similar finding at the Fe/BTO interface.

Table 1 shows the relative displacements of the Fe, Ti, and Pb/Ba atoms with respect to the O-plane at the interface for ferroelectric polarization pointing down P_{\downarrow} and pointing up P_{\uparrow} toward the Fe layers. For P_{\downarrow} , while the magnitude of Ti−O spacing almost remains the same as that of 0.52 (0.18 Å) in bulk PTO (BTO), Ti−O displacement is significantly reduced for P_{\uparrow} due to the presence of the Fe overlayers. The similar phenomenon is also found for Pb/Ba−O displacement. Here, P_{\downarrow} or P_{\uparrow} is determined by the sign of Ti−O (same for Pb/Ba−O) separation, where positive (negative) Ti−O indicates the Ti displacement toward (away from) Fe. The optimized Fe−O at the Fe/PTO interface alters from 1.89 to 2.07 Å upon the polarization reversal, while the corresponding Fe−O displacement at the Fe/BTO interface is insignificant (from 1.93 to

1.92 Å). The former value is notably smaller than that (2.145 Å) in bulk FeO.²⁹ Thus, for P_{\downarrow} , substantial interface effects of the electric depolarization^{1–3,8,30} and orbital hybridization between the Fe 3d and O 2p states^{31,32} are expected, as addressed in the following paragraphs.

In Table 1 we present the absolute values of the calculated local polarization along the z axis (P_z) at the interface for Fe/ PTO and Fe/BTO, respectively, in comparison with the present theoretical and experimental values of bulk PTO and BTO.33,34 The Berry phase approach is adopted for determining the electronic contribution to the polarization.³⁵ For bulk PTO and BTO, the overall agreement between the present theory and experiments is satisfactory; $P_z = 88.7$ and 83 μ C cm⁻² for PTO and P_z = 28.9 and 26 μ C cm⁻² for BTO, respectively. For both Fe/PTO and Fe/BTO, the interfacial local polarization is asymmetric under polarization switching due to the broken crystal inversion symmetry, associated with Ti-O and Pb/Ba-O displacements, and is smaller than that of the bulk (or center layers), particularly for P_{\uparrow} . The interface polarizations of Fe/PTO are 0.50 μC cm⁻² for P_{\downarrow} and 0.32 μC cm⁻² for P_{\uparrow} , which are roughly three times larger than those (0.16 and 0.07 μ C cm⁻²) of Fe/BTO.

Significance of the magnetoelectric coupling is justified with changes in the magnetic moment (ΔM) and relative charge (ΔQ) with respect to the nominal charge upon the ferroelectric polarization reversal. The nominal charges of the Fe, Ti, Pb/Ba, and O atoms in their ground state phases are 8, 4, 2/8, and 6 e, respectively. The absolute values of the interface magnetic moment and charge are given in Table 2. The calculated ΔM and ΔQ are more notable in Fe/PTO than in Fe/BTO: $\Delta M(\text{Fe}) = 0.39 \text{ vs } 0.15 \mu_B$, $\Delta M(\text{Ti}) = 0.58 \text{ vs } 0.62$ $\mu_{\rm B}$, $\Delta M({\rm Pb/Ba}) = -0.02$ vs 0 $\mu_{\rm B}$, and $\Delta M({\rm O}) = 0.05$ vs 0.02 $\mu_{\rm B}$; $\Delta Q({\rm Fe}) = -0.37 \text{ vs } -0.1 \text{ e}$, $\Delta Q({\rm Ti}) = -0.32 \text{ vs } -0.18 \text{ e}$, $\Delta Q(Pb/Ba) = -0.22 \text{ vs } -0.01 \text{ e, and } \Delta Q(O) = -0.18 \text{ vs}$ -0.02 e. For both Fe/PTO and Fe/BTO, those at the other sites away from the interface are negligible. The underlying mechanism for the electric-field induced changes in magnetism has been well established by previous studies in connection with the charge screening and orbital hybridization effects at the interface. 1,7-10

To understand the polarization reversal induced change in magnetism, we show the partial electronic density of states (PDOS) of the Fe 3d-orbital states at the Fe/PTO interface in Figure 2 for P_{\downarrow} (left) and P_{\uparrow} (right panels). In Figure 2, we also

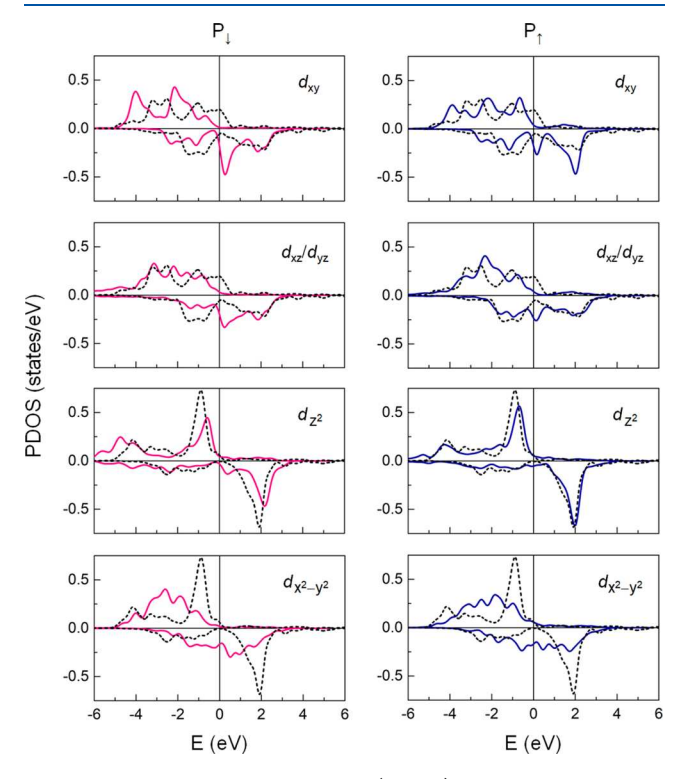


Figure 2. Projected density of states (PDOS) of the Fe atom at the Fe/PTO interface (n = 5) for the ferroelectric polarization down P_{\downarrow} (red solid line in the left panel) and polarization up P_{\uparrow} (blue solid line in the right panel). For comparison, the corresponding PDOS for bulk Fe is also shown in black dashed line. The Fermi level is set to zero in energy.

present the corresponding PDOS for bulk Fe, where the cubic symmetry splits the 3d-orbital states into doublets (e_g) and triplets (t_{2g}) . In the reduced symmetry, the e_g and t_{2g} states split into two singlets a_1 $(d_{x^2-y^2})$ and b_1 (d_z^2) and one singlet b_2 (d_{xy})

and one doublet e ($d_{xz,yz}$), respectively. However, in the presence of the TiO₂ interface states, such a simple crystal field splitting affects not only the absolute value of the 3d energy levels but also the hybridization between the Fe 3d and the O 2p orbital states does. Obviously, unlike bulk Fe, the spin-up states of the interface Fe are completely filled, while the spin-down t_{2g} states are more unoccupied for both P_{\downarrow} and P_{\uparrow} . From this, the charge transfer from Fe to O and Pb (Table 2) occurs mainly in the spin-down electronic state, which in turn enhances the spin exchange splitting (i.e., magnetic moment) of the interface Fe compared with bulk Fe (2.2 $\mu_{\rm B}$). From Table 2 and Figure 2, the interface Fe depletes less charge to the underneath of the O and Pb atoms in P_{\downarrow} than in P_{\uparrow} . This can again explain the larger magnetic moment of the interface Fe in P_{\downarrow} than that in P_{\uparrow} .

In addition to this typical phenomenon at the FM/FE interface, the Fe/PTO interface exhibits magnetization reorientation upon ferroelectric polarization reversal. In Figure 3a we present the calculated MCA and K_s for Fe/PTO as a function of the number of Fe layers. The corresponding MAE, MAE = MCA + K_s , are shown in Figure 3b. As shown in Figure 3a, the saturation behavior of MCA is evident as the number of Fe layers increases beyond n = 5 or 0.6 nm thick, which is within the typical thickness range (0.5-1.2 nm) of the perpendicularly magnetized free layer in spintronic devices.³⁶ Notably, MCA changes sign from positive to negative as the polarization switches from P_{\downarrow} to P_{\uparrow} . The numerical values of MCA (K_s) for Fe/PTO with n = 5 are 0.91 (-0.27) erg/cm² for P_{\perp} and $-0.70~(-0.21)~{\rm erg/cm^2}$ for P_{\uparrow} . The similar $K_{\rm s}$ of -0.27 erg/cm² is reported for the Fe(001) surface.³⁷ From Figure 3a,b, the overall trends of MAE almost resemble those of MCA for both P_{\downarrow} and P_{\uparrow} . This indicates that the magnetization can be reoriented by an electric-field alone without the need for a magnetic-field or spin-polarized electron current. The magnetization reorientation does not occur at the Fe/BTO interface as reported in previous calculations. 1,2,7,8 Such an electric-field assisted magnetization switching is worth noting from a practical viewpoint, which overcomes the major drawbacks of high power consumption in current memory technologies (e.g., STT).6 Nevertheless, we remind readers that the shape anisotropy is always negative and decreases with Fe-film thickness, which is predicted to result in an in-plane

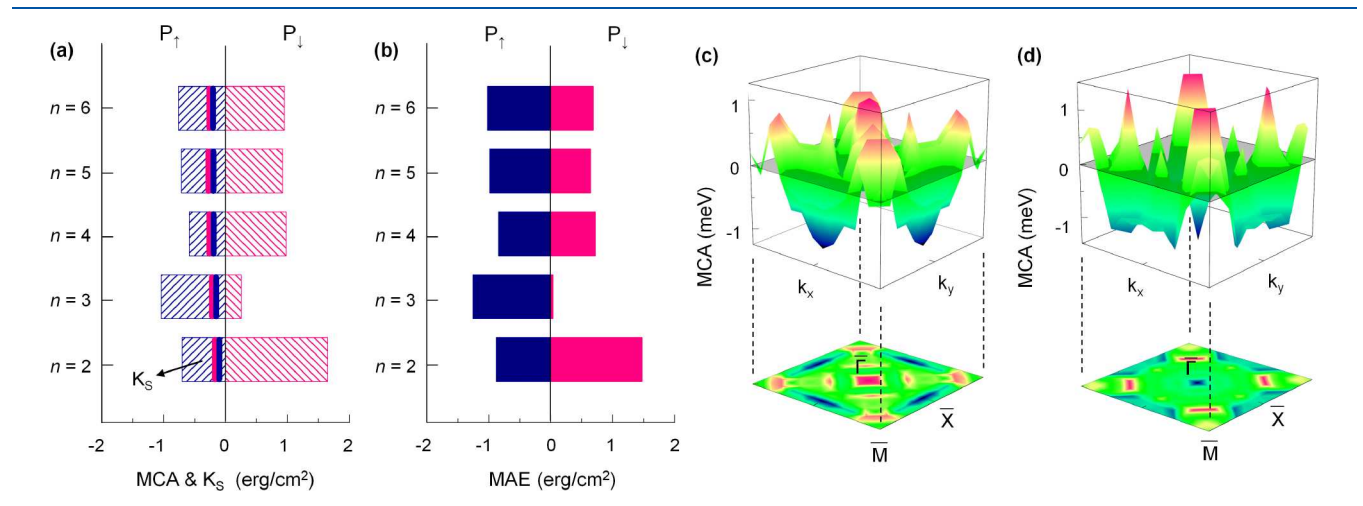


Figure 3. (a) Magnetocrystalline anisotropy MCA (shaded bar) and shape anisotropy K_s (line) and (b) magnetic anisotropy energy MAE of the Fe/PTO heterostructure for different thicknesses n of Fe layers for the ferroelectric polarization down P_{\downarrow} (red) and polarization up P_{\uparrow} (blue). MCA distribution of the Fe/PTO with n = 5 over k space for (c) P_{\downarrow} and (d) P_{\uparrow} . The energy scale in the bar is in units of meV.

magnetization for a thicker Fe-film (critical thickness can be determined by the competition between MCA and K_s) on PTO regardless of the ferroelectric polarization.

We present the k-resolved MCA in Figure 3c for P_{\downarrow} and Figure 3d for P_{\uparrow} using the force theorem: 38 MCA = $\sum_{\mathbf{k}}$ MCA_k, where MCA_k = $\sum_{o} [\varepsilon(n,\mathbf{k})^{\parallel} - \varepsilon(n,\mathbf{k})^{\perp}]$. Here, $\varepsilon(n,\mathbf{k})^{\parallel}$ and $\varepsilon(n,\mathbf{k})^{\perp}$ are the eigenvalues of occupied states in the Hamiltonian for in-plane and perpendicular magnetization, respectively. The MCA values of Fe/PTO (n=5) calculated from the force theorem are 0.98 and -0.69 erg/cm² for P_{\downarrow} and P_{\uparrow} , respectively, which fairly reproduce those (0.91 and -0.70 erg/cm²) obtained by the total energy calculations. The MCA $(\overline{\Gamma})$ resembles MCA in sign upon $P_{\downarrow} \rightarrow P_{\uparrow}$. Positive (negative) contributions to MCA at general k points compensate negative (positive) MCA(k) around \overline{X} (\overline{M}) for P_{\downarrow} (P_{\uparrow}).

In order to understand the magnetization reorientation, we analyze the atom-by-atom decomposition of the SOC energy difference for in-plane and out-of-plane magnetization, $\Delta E_{\rm soc} = E_{\rm soc}^{\parallel} - E_{\rm soc}^{\perp}$ in Figure 4a. Here,

$$E_{\text{soc}} = \left\langle \frac{\hbar^2}{2m^2c^2} \frac{1}{r} \frac{\text{d}V(r)}{\text{d}r} \mathbf{L} \cdot \mathbf{S} \right\rangle$$

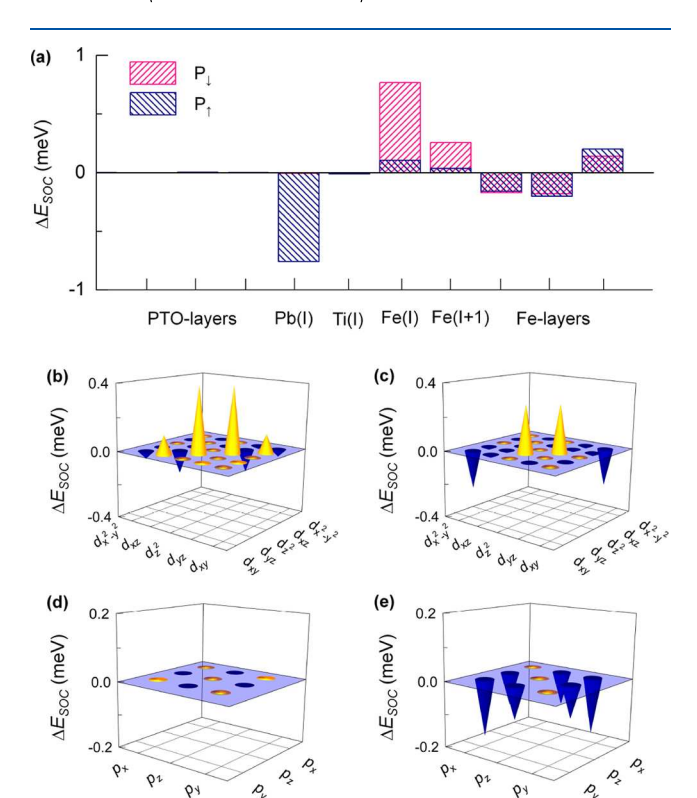


Figure 4. (a) Atom resolved SOC energy difference $\Delta E_{\rm soc}$ of the Fe/PTO layers with n=5 for P_{\downarrow} (red) and P_{\uparrow} (blue bars). Letter I denotes the interface. Orbital resolved $\Delta E_{\rm soc}$ of the Fe and Pb atoms at the interface for (b) and (d) P_{\downarrow} and (c) and (e) P_{\uparrow} . Yellow and blue peaks represent the positive and negative $\Delta E_{\rm soc}$ values, respectively.

where V(r) is the spherical part of the effective potential within the PAW scheme, and L and S are orbital and spin operators, respectively. The expectation value of $E_{\rm soc}$ is twice the actual value of the total energy correction to the second order in SOC, i.e., MCA $\approx {}^{1}/{}_{2}\Delta E_{\rm soc}$. The other 50% of the SOC energy translates into the crystal-field energy and the formation of the unquenched orbital moment. Al,42 Note that the sum of

the atom-resolved contributions obtained from the SOC energy calculations is in reasonable agreement (within 5%) with those obtained from total energy calculations. As shown in Figure 4a, MCA change upon polarization reversal is exclusive for the interface layers, including Fe(I), Fe(I+1), and Pb(I) (which are indicated in Figure 1a), whereas those of the center layers in Fe and PTO are rather small. Previous calculations reported that Fe exhibits larger PMA when in contact with the oxide surface through the p_z – d_z ² hybridization. This is also the case for Fe/PTO when P_{\downarrow} ; PMA comes from the Fe(I) and Fe(I+1) layers. While these PMA concentrations are reduced greatly for P_{\uparrow} , Pb(I) provides a large contribution to negative MCA.

We further decompose $\Delta E_{\rm soc}$ into Fe(I) 3d and Pb(I) 6p orbital contributions in parts b and d of Figure 4 for P_{\downarrow} and in parts c and e of Figure 4 for P_{\uparrow} , respectively. The corresponding band structures of Fe(I) and Pb(I) are also shown in Figure 5a–d. From Figure 4b, PMA is predominated

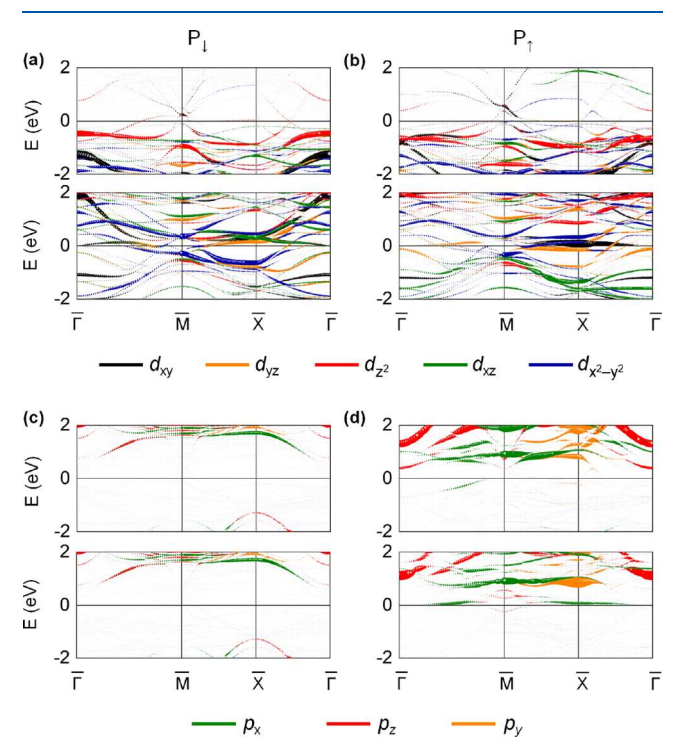


Figure 5. Spin-up (upper) and spin-down (bottom) electronic band structure of the Fe and Pb atoms at the Fe/PTO interface for the (a) and (c) ferroelectric polarization down P_{\downarrow} and (b) and (d) polarization up P_{\uparrow} . In (a) and (b), the black, orange, green, red, and blue lines denote the d_{xy} , d_{xz} , d_{yz} , d_{z}^2 , and $d_{x^2-y^2}$ orbital characters, respectively. In (c) and (d), the green, red, and orange lines represent the p_{xy} , p_{zy} and p_{y} orbital characters, respectively. The size of the symbols represents the weight of the orbital states. The Fermi level is set to zero in energy.

by the matrix element $\langle xz,yz_\uparrow|\hat{L}_z|z_\downarrow^2\rangle$ according to the perturbation theory,⁴³ where $\hat{L}_{z(x)}$ is the z(x) component of the orbital angular momentum operator. Here, subscripts \uparrow and \downarrow denote spin-up and spin-down state, respectively. As Ti displaces toward the interface Fe, the strong $p_z-d_{z^2}$ hybridization weakens because of the enlarged Fe–O displacement, which in turn reduces PMA. Consequently, the intrinsic feature of small MCA in Fe(001) can most likely be preserved. Since the d z^2 band above the Fermi level in the spin-down state

Table 3. Relative Displacement (Å) of the Fe, Ti, and Pb with Respect to the O-Plane, Magnetic Moment (μ_B), and MCA (meV) of the Fe, Ti, and Pb Atoms at the Fe/PTO Interface for Different Strains of -1%, 0%, and 1% for the Ferroelectric Polarization Down P_{\downarrow} and Polarization Up P_{\uparrow}^{a}

					magnetic moment			MCA				
		Fe-O	Ti-O	Pb-O	Fe	Ti	Pb	Fe	Ti	Pb	$K_{\rm s}$	MAE
-1	P_{\downarrow}	1.90	0.53	0.85	2.85	0.04	0.00	0.38	-0.01	-0.01	-0.27	0.08
	P_{\uparrow}	2.08	0.35	0.63	2.46	-0.50	0.02	0.04	-0.02	-0.78	-0.22	-1.18
0	P_{\downarrow}	1.89	0.51	0.83	2.85	0.04	0.00	0.38	-0.01	-0.01	-0.27	0.64
	P_{\uparrow}	2.07	0.34	0.60	2.46	-0.54	0.02	0.05	-0.01	-0.76	-0.21	-0.91
1	P_{\downarrow}	1.88	0.46	0.71	2.84	0.04	0.00	0.39	0.00	0.00	-0.27	0.81
	P_{\uparrow}	2.04	0.29	0.57	2.50	-0.55	0.03	0.05	-0.01	-0.72	-0.20	-0.43
a -			_			,			_			

^aThe surface shape anisotropy K_s and magnetic anisotropy energy MAE (erg/cm²) of the system are also presented.

shifts upward away from the Fermi level as $P_{\downarrow} \to P_{\uparrow}$ (Figures 2 and 4), the aforementioned SOC pairing term with the empty d_z^2 state is largely limited. Meanwhile, the spin-up d_{xy} state appears around -1 eV at $\overline{\Gamma}$, which can couple with the unoccupied spin-down $d_{x^2-y^2}$ state, as shown in Figure 5. Thus, negative contribution of the $\langle xy_{\uparrow}|\hat{L}_x|x^2-y_{\downarrow}^2\rangle$ coupling becomes comparable to positive contribution by the $\langle xz,yz_{\uparrow}|\hat{L}_z|z_{\downarrow}^2\rangle$ (Figure 4c). From Figure 5c,d, the Pb 6p bands move downward across the Fermi level upon $P_{\downarrow} \to P_{\uparrow}$, and the spinbands of them are no longer degenerate. This indicates that the Pb 6p orbitals accumulate more charges in P_{\uparrow} than in P_{\downarrow} , as addressed in Table 2. We assign that for P_{\uparrow} these p_x/p_y states around the Fermi level at $\overline{\Gamma}$ should be involved for SOC pairs that lead to negative $\Delta E_{\rm soc}$ in Figure 4e.

We finally explore the strain effect, which should not be excluded because of the Rashba spin-orbit coupling. The Rashba spin-orbit coupling is proportional to the net electricfield from both the internal and external fields at the interface.44 In particular, the Rashba splitting of the band structure is very sensitive to the strain effect. 45 Both the compressive and tensile strains (η) of $\pm 1\%$ are imposed into the in-plane lattice of PTO layers, where $\eta = [(a_{\parallel} - a_0)/a_0] \times$ 100%, a_{\parallel} and a_0 are variable and equilibrium in-plane lattice constants, respectively. Table 3 presents the calculated displacement, magnetic moment, and MCA of the Fe, Ti, and Pb atoms at the Fe/PTO interface for $\eta = \pm 1\%$. As expected, all Fe-O, Ti-O, and Pb-O displacements increase (decrease) with the compressive (tensile) strain. The magnetic moments of the interface Fe, Ti, and Pb atoms retain nearly the same under strain. It is found from MCA and K_s that MAE = 0.08 (0.81) erg/cm² for P_{\downarrow} and = -1.18 (-0.43) erg/cm² for P_{\uparrow} at $\eta = -1$ (1)%. From this, one can expect that strains more than ±2%, particularly the compressive strain, might not be desirable for magnetization switching although $\eta \geq \pm 2\%$ is not practical. On the other side, this drastic sensitivity of MAE to the strain effect suggests another viewpoint: possible magnetization switching at the Fe/BTO interface if an epitaxial strain is addressed properly.² However, one needs to be more careful regarding the strength of the internal and external electric fields, which must be sufficient to minimize the Fe 3d-O 2p hybridization. Recent experiments support the scenario in which the presence of highly electric-polarized Pb-(Mg_{1/3}Nb_{2/3})_{0.7}Ti_{0.3}O₃ (PMN-PT) is indispensable for magnetization switching in CoFeB/PMN-PT. 11,12

CONCLUSION

In summary, using the DFT and DFPT calculations, we have predicted magnetization reorientation at the thermodynamically stable interface between the Fe(001) and PbTiO₃(001) layers by the ferroelectric polarization reversal. The underlying mechanism for the anisotropic phenomenon is discussed with the energy level changes of the interface Fe 3d and Pb 6p orbital states in the spin-orbit Hamiltonian matrix elements through the ferroelectric polarization reversal induced changes of the Fe-O and Ba-O plane separations and the corresponding orbital hybridizations. This magnetization reversal persists for Fe-film thicknesses of more than 1 nm and even under a practically achievable strain of 1%. The present study would suggest that the Fe/PbTiO₃ interface can act as a prototype bilayer heterostructure for a practical magnetoelectric interface with the electric-field switchable magnetization in spintronic applications.

AUTHOR INFORMATION

Corresponding Author

Dorj Odkhuu — Department of Physics, Incheon National University, Incheon 22012, South Korea; ⊚ orcid.org/0000-0002-2184-024X; Email: odkhuu@inu.ac.kr

Authors

Tumentsereg Ochirkhuyag — Department of Physics, Incheon National University, Incheon 22012, South Korea;
orcid.org/0000-0002-3044-7589

Nicholas Kioussis — Department of Physics, California State University, Northridge, California 91330, United States Sonny H. Rhim — Department of Physics, University of Ulsan, Ulsan 44610, South Korea

Complete contact information is available at: https://pubs.acs.org/10.1021/acs.jpcc.3c06812

Notes

The authors declare no competing financial interest.

ACKNOWLEDGMENTS

This work was supported by Incheon National University Research Grant in 20210418. N.K. acknowledges support from NSF-PREM Grant number DMR-1828019.

REFERENCES

(1) Duan, C. G.; Jaswal, S. S.; Tsymbal, E. Y. Predicted magnetoelectric effect in Fe/BaTiO $_3$ multilayers: Ferroelectric control of magnetism. *Phys. Rev. Lett.* **2006**, *97*, 047201.

- (2) Odkhuu, D.; Kioussis, N. Strain-driven electric control of magnetization reversal at multiferroic interfaces. *Phys. Rev. B* **2018**, 97, 094404.
- (3) Odkhuu, D. Electric control of magnetization reorientation in FeRh/BaTiO₃ mediated by a magnetic phase transition. *Phys. Rev. B* **2017**, *96*, 134402.
- (4) Eerenstein, W.; Mathur, N. D.; Scott, J. F. Multiferroic and magnetoelectric materials. *Nature* **2006**, 442, 759.
- (5) Bibes, M.; Barth él émy, A. Towards a magnetoelectric memory. *Nat. Mater.* **2008**, *7*, 425.
- (6) Slonczewski, J. C. Conductance and exchange coupling of two ferromagnets separated by a tunneling barrier. *Phys. Rev. B* **1989**, 39, 6995
- (7) Duan, C. G.; Velev, J. P.; Sabirianov, R. F.; Mei, W. N.; Jaswal, S. S.; Tsymbal, E. Y. Tailoring magnetic anisotropy at the ferromagnetic/ferroelectric interface. *Appl. Phys. Lett.* **2008**, *92*, 122905.
- (8) Fechner, M.; Maznichenko, I. V.; Ostanin, S.; Ernst, A.; Henk, J.; Bruno, P.; Mertig, I. Magnetic phase transition in two-phase multiferroics predicted from first principles. *Phys. Rev. B* **2008**, 78, 212406.
- (9) Fechner, M.; Maznichenko, I. V.; Ostanin, S.; Ernst, A.; Henk, J.; Mertig, I. Ab initio study of magnetoelectricity in composite multiferroics. *Phys. Status Solidi B* **2010**, 247, 1600.
- (10) Radaelli, G.; Petti, D.; Plekhanov, E.; Fina, I.; Torelli, P.; Salles, B. R.; Cantoni, M.; Rinaldi, C.; Gutiérrez, D.; Panaccione, G.; et al. Electric control of magnetism at the Fe/BaTiO₃ interface. *Nat. Commun.* **2014**, *5*, 3404.
- (11) Li, P.; Chen, A.; Li, D.; Zhao, Y.; Zhang, S.; Yang, L.; Liu, Y.; Zhu, M.; Zhang, H.; Han, X. Electric field manipulation of magnetization rotation and tunneling magnetoresistance of magnetic tunnel junctions at room temperature. *Adv. Mater.* **2014**, *26*, 4320.
- (12) Peng, R. C.; Wang, J. J.; Hu, J. M.; Chen, L. Q.; Nan, C. W. Electric-field-driven magnetization reversal in square-shaped nanomagnet-based multiferroic heterostructure. *Appl. Phys. Lett.* **2015**, *106*, 142901.
- (13) Wei, L. Y.; Lian, C.; Meng, S. Prediction of two-dimensional electron gas mediated magnetoelectric coupling at ferroelectric PbTiO₃/SrTiO₃ heterostructures. *Phys. Rev. B* **2017**, *95*, 184102.
- (14) Kresse, G.; Furthmüller, J. Efficient iterative schemes for ab initio total-energy calculations using a plane-wave basis set. *Phys. Rev.* B **1996**, *54*, 11169.
- (15) Kresse, G.; Furthmüller, J. Efficiency of ab initio total energy calculations for metals and semiconductors using a plane-wave basis set. *Comput. Mater. Sci.* **1996**, *6*, 15.
- (16) Perdew, J. P.; Burke, K.; Ernzerhof, M. Generalized gradient approximation made simple. *Phys. Rev. Lett.* **1996**, *77*, 3865.
- (17) Rodriguez, J. A.; Etxeberria, A.; González, L.; Maiti, A. Structural and electronic properties of PbTiO₃, PbZrO₃, and PbZr_{0.5}Ti_{0.5}O₃: First-principles density-functional studies. *J. Chem. Phys.* **2002**, *117*, 2699.
- (18) Petraru, A.; Pertsev, N. A.; Kohlstedt, H.; Poppe, U.; Waser, R.; Solbach, A.; Klemradt, U. Polarization and lattice strains in epitaxial BaTiO₃ films grown by high-pressure sputtering. *J. Appl. Phys.* **2007**, *101*, 114106.
- (19) Meyerheim, H. L.; Klimenta, F.; Ernst, A.; Mohseni, K.; Ostanin, S.; Fechner, M.; Parihar, S.; Maznichenko, I. V.; Mertig, I.; Kirschner, J. Structural secrets of multiferroic interfaces. *Phys. Rev. Lett.* **2011**, *106*, 087203.
- (20) Fechner, M.; Zahn, P.; Ostanin, S.; Bibes, M.; Mertig, I. Switching magnetization by 180° with an electric field. *Phys. Rev. Lett.* **2012**, *108*, 197206.
- (21) Koelling, D. D.; Harmon, B. N. A technique for relativistic spin-polarised calculations. *J. Phys. C: Solid State Phys.* 1977, 10, 3107.
- (22) Bruno, P. Physical origins and theoretical models of magnetic anisotropy. In *Magnetismus von Festkorpern und Grenzflochen*; Forschungszentrum Julich: Julich, Germany, 1993; Vol. 24, pp 1–28.
- (23) Togo, A.; Tanaka, I. First principles phonon calculations in materials science. Scr. Mater. 2015, 108, 1.

- (24) Giannozzi, P.; de Gironcoli, S.; Pavone, P.; Baroni, S. Ab initio calculation of phonon dispersions in semiconductors. *Phys. Rev. B* **1991**, 43, 7231.
- (25) Grabowski, B.; Hickel, T.; Neugebauer, J. Ab initio study of the thermodynamic properties of nonmagnetic elementary fcc metals: Exchange-correlation-related error bars and chemical trends. *Phys. Rev. B* **2007**, *76*, 024309.
- (26) Mediukh, N. R.; Ivashchenko, V. I.; Pogrebnjak, D. A.; Shevchenko, V. I. First-principles study of thermodynamic and stability properties of TiC-SiC alloys. *Proceedings*, 6th International Conference. Nanomaterials: Applications and Properties, 2016; Sumy State University, 2016; 01NTF14.
- (27) Lazewski, J.; Korecki, J.; Parlinski, K. Phonons of (100) and (110) iron surfaces from first-principles calculations. *Phys. Rev. B* **2007**, 75, 054303.
- (28) Ślęzak, T.; Łazewski, J.; Stankov, S.; Parlinski, K.; Reitinger, R.; Rennhofer, M.; Rüffer, R.; Sepiol, B.; Ślęzak, M.; Spiridis, N.; et al. Phonons at the Fe(110) Surface. *Phys. Rev. Lett.* **2007**, *99*, 066103.
- (29) Meyerheim, H. L.; Popescu, R.; Jedrecy, N.; Vedpathak, M.; Sauvage-Simkin, M.; Pinchaux, R.; Heinrich, B.; Kirschner, J. Surface x-ray diffraction analysis of the MgO/Fe(001) interface: Evidence for an FeO layer. *Phys. Rev. B* **2002**, *65*, 144433.
- (30) Qurat-ul-ain; Odkhuu, D.; Rhim, S. H.; Hong, S. C. Enhanced voltage-controlled magnetic anisotropy via magnetoelasticity in FePt/MgO(001). *Phys. Rev. B* **2020**, *101*, 214436.
- (31) Yang, H. X.; Chshiev, M.; Dieny, B.; Lee, J. H.; Manchon, A.; Shin, K. H. First-principles investigation of the very large perpendicular magnetic anisotropy at Fe/MgO and Co/MgO interfaces. *Phys. Rev. B* **2011**, *84*, 054401.
- (32) Odkhuu, D.; Tsevelmaa, T.; Sangaa, D.; Tsogbadrakh, N.; Rhim, S. H.; Hong, S. C. First-principles study of magnetization reorientation and large perpendicular magnetic anisotropy in CuFe₂O₄/MgO heterostructures. *Phys. Rev. B* **2018**, *98*, 094408.
- (33) Liu, Y.; Zhu, Y.-L.; Tang, Y.-L.; Wang, Y.-J.; Jiang, Y.-X.; Xu, Y.-B.; Zhang, B.; Ma, X.-L. Local enhancement of polarization at PbTiO₃/BiFeO₃ interfaces mediated by charge transfer. *Nano Lett.* **2017**, *17*, 3619.
- (34) Jaffe, B.; Cook, W. R., Jr.; Jaffe, H. Piezoelectric Ceramics; Academic Press: London, 1971; p 78.
- (35) King-Smith, R. D.; Vanderbilt, D. Theory of polarization of crystalline solids. *Phys. Rev. B* **1993**, *47*, 1651.
- (36) Ikeda, S.; Miura, K.; Yamamoto, H.; Mizunuma, K.; Gan, H. D.; Endo, M.; Kanai, S.; Hayakawa, J.; Matsukura, F.; Ohno, H. A perpendicular-anisotropy CoFeB—MgO magnetic tunnel junction. *Nat. Mater.* **2010**, *9*, 721.
- (37) Ohnishi, S.; Weinert, M.; Freeman, A. J. Interface magnetism in metals: Ag/Fe(001). *Phys. Rev. B* **1984**, *30*, *36*.
- (38) Weinert, M.; Watson, R. E.; Davenport, J. W. Total-energy differences and eigenvalue sums. *Phys. Rev. B* 1985, 32, 2115.
- (39) Antropov, V.; Ke, L.; Aberg, D. Constituents of magnetic anisotropy and a screening of spin-orbit coupling in solids. *Solid State Commun.* **2014**, *194*, 35.
- (40) Zhang, J.; Lukashev, P. V.; Jaswal, S. S.; Tsymbal, E. Y. Model of orbital populations for voltage-controlled magnetic anisotropy in transition-metal thin films. *Phys. Rev. B* **2017**, *96*, 014435.
- (41) Skomski, R.; Kashyap, A.; Enders, A. Is the magnetic anisotropy proportional to the orbital moment? *J. Appl. Phys.* **2011**, *109*, 07E143. (42) Odkhuu, D.; Hong, S. C. First-Principles Prediction of Possible
- (42) Odkhuu, D.; Hong, S. C. First-Principles Prediction of Possible Rare-Earth Free Permanent Magnet of Tetragonal FeCo with Enhanced Magnetic Anisotropy and Energy Product through Interstitial Nitrogen. *Phys. Rev. Appl.* **2019**, *11*, 054085.
- (43) Wang, D. S.; Wu, R.; Freeman, A. J. First-principles theory of surface magnetocrystalline anisotropy and the diatomic-pair model. *Phys. Rev. B* **1993**, *47*, 14932.
- (44) Barnes, S. E.; Ieda, J.; Maekawa, S. Rashba spin-orbit anisotropy and the electric field control of magnetism. *Sci. Rep.* **2014**, *4*, 4105.
- (45) Ong, P. V.; Kioussis, N.; Odkhuu, D.; Amiri, P. K.; Wang, K. L.; Carman, G. P. Giant voltage modulation of magnetic anisotropy in

strained heavy metal/magnet/insulator heterostructures. *Phys. Rev. B* 2015, 92, 020407.